Pergamon

Int. J. Solids Structures Vol. 34, No. 29, pp. 3781–3794, 1997

0020–7683/97 $17.00 + .00

PII: S0020–7683(97)00009–7

A NOTE ON THE STATIC BEHAVIOR OF SIMPLY-SUPPORTED LAMINATED PIEZOELECTRIC CYLINDERS

PAUL HEYLIGER
Department of Civil Engineering, Colorado State University, Fort Collins CO 80523, U.S.A.

(*Received* 9 *April* 1996; *in revised form* 27 *November* 1996)

Abstract—An exact three-dimensional solution of the equations of linear piezoelectricity is given for the static response of a finite laminated piezoelectric cylinder with its ends simply supported. The equilibrium equations and the conservation of charge equation are constructed in cylindrical coordinates. The three displacement components and the electrostatic potential are expressed in terms of Fourier series in the axial and circumferential directions, leading to a coupled system of four ordinary differential equations in the radial coordinate. The Frobenious method is used to obtain the elastic and electric fields for each layer of the laminate, which are a function of eight constants. Enforcing the boundary and continuity conditions across each interface yields the required number of equations to solve for these constants. Several examples are presented to study the fundamental behavior of these solids. © 1997 Elsevier Science Ltd.

INTRODUCTION

Exact solutions for laminated piezoelectric solids provide a very useful means of comparison for developing more efficient and computationally powerful approximate beam, plate, shell, and continuum models. In piezoelectric solids, the electric and elastic fields are coupled through the constitutive relations, leading to significantly different behavior than purely elastic laminates.

Exact solutions for simply-supported, laminated piezoelectric plates have been obtained by Ray and co-workers (1993), Heyliger (1994), Heyliger and Brooks (1995), Heyliger and Saravanos (1995), and Xu and co-workers (1995). There have been a number of studies of laminated piezoelectric cylinders, including those documented and described in the books of Parton and Kudryavtsev (1988) and Tzou (1993). Others include the two-dimensional vibration study of Adelman and Stavsky (1975), the studies on wave propagation by Sun and Cheng (1974) using analytic techniques and by Siao *et al.* (1994) using a finite element method, and the study of static behavior using an approximate theory by Mitchell and Reddy (1995). Paul and Natarajan (1996) examined flexural vibrations of hollow cylinders of class 6 mm using a separation of variables techniques that resulted in small but finite errors in satisfying the boundary and surface conditions of the cylinder.

Srinivas (1974) has presented an exact elasticity solution for the response of simply-supported elastic laminates using the Frobenious method to solve the ordinary differential equations in the radial variable. In this note, the methodology of Srinivas is extended to include the effects of laminated cylinders composed either entirely or in part of piezoelectric layers. In addition to the conditions on the displacements and stresses, the necessary conditions on the electrostatic potential and electric displacement must be enforced. This note differs from previous work on piezoelectric cylinders in that the case of simple support is studied and that the analysis is exact as all boundary and surface conditions are satisfied as well as the governing differential equations.

The solution is constructed for the static three-dimensional response of these cylinders. The methodology is used to consider the fundamental behavior of these problems, including the nature of the potential variation through the thickness and the influence of the shell length/thickness ratio on the elastic and electric fields.

GEOMETRY AND BOUNDARY CONDITIONS

A circular cylinder is composed of M layers of elastic or piezoelectric material. The principal geometrical directions of the cylinder align with those of the cylindrical coordinate system (r, θ, z) and the three displacements associated with these directions are denoted as u_r, u_θ, and u_z. The electrostatic potential is denoted by ϕ. The length of the cylinder in the axial direction z is L. The cylinder is hollow, with the inner radius defined as R_I and the outer radius R_O. The innermost layer with respect to the radius is defined as layer 1, with the outmost layer defined as layer M. The radial position of the interface between the layer i and layer $(i+1)$ is defined as R_i. The total wall thickness in the radial direction is $R_O - R_I = H$.

The boundary conditions at the faces normal to the z axis at $z = 0$ and $z = L$ are those typically associated with the conditions of simple support combined with the electrical condition that the end faces are grounded. Hence, at these locations, the following conditions exist:

$$u_r^i = u_\theta^i = \sigma_{zz}^i = \phi^i = 0 \tag{1}$$

where σ_{zz} is the normal axial stress and the i superscript denotes the variable for a given layer. On the radial faces $r = R_I$ and $r = R_O$ the boundary conditions are more arbitrary and are discussed in the sequel. Each layer of the laminate is treated as a homogeneous piezoelectric layer with orthorhombic symmetry. The piezoelectric layers have been poled in the radial direction.

The three equations of equilibrium are given by (Fung 1965)

$$\frac{1}{r}\frac{\partial}{\partial r}(r\sigma_{rr}) + \frac{1}{r}\frac{\partial \sigma_{r\theta}}{\partial \theta} + \frac{\partial \sigma_{rz}}{\partial z} - \frac{\sigma_{\theta\theta}}{r} = 0 \tag{2}$$

$$\frac{1}{r^2}\frac{\partial}{\partial r}(r^2\sigma_{r\theta}) + \frac{1}{r}\frac{\partial \sigma_{\theta\theta}}{\partial \theta} + \frac{\partial \sigma_{\theta z}}{\partial z} = 0 \tag{3}$$

$$\frac{1}{r}\frac{\partial}{\partial r}(r\sigma_{rz}) + \frac{1}{r}\frac{\partial \sigma_{\theta z}}{\partial \theta} + \frac{\partial \sigma_{zz}}{\partial z} = 0. \tag{4}$$

The charge equation of electrostatics is given by (Tiersten 1969)

$$\frac{1}{r}\frac{\partial}{\partial r}(rD_r) + \frac{1}{r}\frac{\partial D_\theta}{\partial \theta} + \frac{\partial D_z}{\partial z} = 0. \tag{5}$$

The strain-displacement relations are given by

$$S_1 = \varepsilon_{rr} = \frac{\partial u_r}{\partial r} \quad S_2 = \varepsilon_{\theta\theta} = \frac{1}{r}\frac{\partial u_\theta}{\partial \theta} + \frac{u_r}{r} \quad S_3 = \varepsilon_{zz} = \frac{\partial u_z}{\partial z} \tag{6}$$

$$S_4 = \gamma_{rz} = \frac{\partial u_z}{\partial r} + \frac{\partial u_r}{\partial z} \quad S_5 = \gamma_{r\theta} = \frac{1}{r}\frac{\partial u_r}{\partial \theta} + \frac{\partial u_\theta}{\partial r} - \frac{u_\theta}{r} \quad S_6 = \gamma_{\theta z} = \frac{\partial u_\theta}{\partial z} + \frac{1}{r}\frac{\partial u_z}{\partial \theta} \tag{7}$$

and the field-potential relations are given as

$$E_r = -\frac{\partial \phi}{\partial r} \quad E_\theta = -\frac{1}{r}\frac{\partial \phi}{\partial \theta} \quad E_z = -\frac{\partial \phi}{\partial z}. \tag{8}$$

The constitutive equations can be written in compressed notation as

$$\sigma_p = C_{pq}S_q - e_{kp}E_k$$
$$D_i = e_{iq}S_q + \varepsilon_{ik}E_k. \tag{9}$$

Here p and q take the values $1,\ldots,6$ and i and k take the values $1,\ldots,3$, σ_p are the components of the stress tensor, C_{pq} are the elastic stiffness components at constant electric field, S_q are the components of infinitesimal strain, e_{iq} are the piezoelectric coefficients, E_k are the components of the electric field, D_i are the components of the electric displacement, and ε_{ik} are the dielectric constants at constant strain. The single subscript for the stress components represents the double subscript notation as the corresponding strain components in eqn (6). The rotated elastic stiffnesses are given by C_{11}, C_{22}, C_{33}, C_{44}, C_{55}, C_{66}, C_{12}, C_{13}, and C_{23}. The non-zero piezoelectric coefficients are given as e_{11}, e_{12}, e_{13}, e_{34}, and e_{25}, and the non-zero dielectric constants are ε_{11}, ε_{22}, and ε_{33}.

The solution procedure that follows is based on similar steps outlined by Srinivas (1974); hence identical nomenclature is used here. The primary differences in this note are in the coupling of the elastic and electric field through the constitutive relations and the satisfaction of the charge equation in addition to those of equilibrium

Substituting eqns (6–8) into eqns (2–5) yields four coupled partial differential equations in terms of the three displacements, u_r, u_θ, u_z, and the electrostatic potential ϕ, each of which is a function of (r, θ, z).

The dependence on the circumferential and axial coordinate can be separated by assuming fields of the form

$$u_r^i(r,\theta,z) = \sum_{m=0}^{\infty}\sum_{n=0}^{\infty} \Psi_r^{mn}(r)\cos m\theta \sin\frac{n\pi z}{b} \tag{10}$$

$$u_\theta^i(r,\theta,z) = \sum_{m=0}^{\infty}\sum_{n=0}^{\infty} \Psi_\theta^{mn}(r)\sin m\theta \sin\frac{n\pi z}{b} \tag{11}$$

$$u_z^i(r,\theta,z) = \sum_{m=0}^{\infty}\sum_{n=0}^{\infty} \Psi_z^{mn}(r)\cos m\theta \cos\frac{n\pi z}{b} \tag{12}$$

$$\phi^i(r,\theta,z) = \sum_{m=0}^{\infty}\sum_{n=0}^{\infty} \Psi_\phi^{mn}(r)\cos m\theta \sin\frac{n\pi z}{b}. \tag{13}$$

The superscript mn on the radial functions indicates the specific Fourier harmonic being considered. Substitution of these expressions into the four governing equations yields the ordinary differential equations

$$\left[C_{11}\frac{d^2}{dr^2} + C_{11}\frac{1}{r}\frac{d}{dr} - \frac{1}{r^2}(C_{55}m^2 + C_{22}) - C_{44}N^2\right]\Psi_r^{mn}$$
$$+\left[(C_{12}+C_{55})\frac{m}{r}\frac{d}{dr} - (C_{55}+C_{22})\frac{m}{r^2}\right]\Psi_\theta^{mn}$$
$$+\left[-(C_{44}+C_{13})N\frac{d}{dr} - (C_{13}-C_{23})\frac{N}{r}\right]\Psi_z^{mn}$$
$$+\left[e_{11}\frac{d^2}{dr^2} + \frac{e_{11}}{r}\frac{d}{dr} - e_{25}\frac{m^2}{r^2} - e_{34}N^2 - \frac{e_{12}}{r}\frac{d}{dr}\right]\Psi_\phi^{mn} = 0 \tag{14}$$

$$\left[-(C_{12}+C_{55})\frac{m}{r}\frac{\mathrm{d}}{\mathrm{d}r}-(C_{55}+C_{22})\frac{m}{r^2}\right]\Psi_r^{mn}$$
$$+\left[C_{55}\frac{\mathrm{d}}{\mathrm{d}r^2}-(C_{22}m^2+C_{55})\frac{1}{r^2}-C_{66}N^2+C_{55}\frac{1}{r}\frac{\mathrm{d}}{\mathrm{d}r}\right]\Psi_\theta^{mn}$$
$$+(C_{23}+C_{66})\frac{mn}{r}\Psi_z^{mn}+\left[-e_{25}\frac{m}{r}\frac{\mathrm{d}}{\mathrm{d}r}-e_{25}\frac{m}{r^2}-e_{12}\frac{m}{r}\frac{\mathrm{d}}{\mathrm{d}r}\right]\Psi_\phi^{mn}=0 \quad (15)$$

$$\left[(C_{44}+C_{13})N\frac{\mathrm{d}}{\mathrm{d}r}+(C_{44}+C_{23})\frac{N}{r}\right]\Psi_r^{mn}+\left[(C_{66}+C_{23})\frac{mn}{r}\right]\Psi_\theta^{mn}$$
$$+\left[C_{44}\frac{\mathrm{d}^2}{\mathrm{d}r^2}+C_{44}\frac{1}{r}\frac{\mathrm{d}}{\mathrm{d}r}-C_{66}\frac{m^2}{r^2}-N^2C_{33}\right]\Psi_z^{mn}+\left[e_{34}N\frac{\mathrm{d}}{\mathrm{d}r}+e_{34}\frac{N}{r}+e_{13}N\frac{\mathrm{d}}{\mathrm{d}r}\right]\Psi_\phi^{mn}=0 \quad (16)$$

$$\left[e_{11}\frac{\mathrm{d}^2}{\mathrm{d}r^2}+e_{12}\frac{1}{r}\frac{\mathrm{d}}{\mathrm{d}r}+e_{11}\frac{1}{r}\frac{\mathrm{d}}{\mathrm{d}r}-e_{25}\frac{m^2}{r^2}-e_{34}N^2\right]\Psi_r^{mn}\left[e_{12}\frac{m}{r}\frac{\mathrm{d}}{\mathrm{d}r}+e_{25}\frac{m}{r}\frac{\mathrm{d}}{\mathrm{d}r}-e_{25}\frac{m}{r^2}\right]\Psi_\theta^{mn}$$
$$+\left[-(e_{13}+e_{34})N\frac{\mathrm{d}}{\mathrm{d}r}-e_{13}\frac{N}{r}\right]\Psi_z^{mn}-\left[\varepsilon_{11}\frac{\mathrm{d}^2}{\mathrm{d}r^2}+\frac{\varepsilon_{11}}{r}\frac{\mathrm{d}}{\mathrm{d}r}-\varepsilon_{22}\frac{m^2}{r^2}-\varepsilon_{33}N^2\right]\Psi_\phi^{mn}=0 \quad (17)$$

where $N=n\pi/b$ has been introduced. Solutions for the functions Ψ are assumed in the Frobenious form

$$\{\Psi_r(r);\Psi_\theta(r);\Psi_z(r);\Psi_\phi(r)\}=\sum_{j=0}^{\infty}r^{\alpha+j}\{H_r(j);H_\theta(j);H_z(j);H_\phi(j)\} \quad (18)$$

where the $H(j)$ terms are constants. The radial functions are still dependent on the associated Fourier harmonics m and n, but these are dropped for simplicity and this dependence is assumed. These expressions are then substituted into eqns (13)–(16). Collecting the coefficients of $r^{\alpha-2}$ yields the matrix equation relating the coefficients for $j=0$ as

$$\begin{bmatrix} C_{11}\alpha^2-C_{55}m^2-C_{22} & (C_{55}+C_{12})m\alpha-(C_{55}+C_{22})m & 0 & e_{11}\alpha^2-e_{25}m^2-e_{12}\alpha \\ -(C_{55}+C_{12})m\alpha-(C_{55}+C_{22})m & C_{55}\alpha^2-C_{22}m^2-C_{55} & 0 & -e_{25}m(\alpha+1)-e_{12}m\alpha \\ 0 & 0 & C_{44}\alpha^2-C_{66}m^2 & 0 \\ e_{11}\alpha^2+e_{12}\alpha-e_{25}m^2 & e_{12}m\alpha+e_{25}m\alpha & 0 & -\varepsilon_{11}\alpha^2+\varepsilon_{22}m^2 \end{bmatrix}$$
$$\begin{Bmatrix} H_r(0) \\ H_\theta(0) \\ H_z(0) \\ H_\phi(0) \end{Bmatrix}=\begin{Bmatrix} 0 \\ 0 \\ 0 \\ 0 \end{Bmatrix}. \quad (19)$$

The axial harmonic n does not appear in this initial expression but is contained in recurrence relations for larger values of j.

A nontrivial solution is obtained if the determinant of this matrix is equal to zero. This results in an eighth-order polynomial in α, two roots of which are

$$\alpha_{7,8}=\pm\sqrt{\frac{C_{66}}{C_{44}}}m. \quad (20)$$

After these roots are factored out, the resulting sixth-order polynomial is written as

$$a_1\alpha^6 + a_2\alpha^4 + a_3\alpha^2 + a_4 = 0. \tag{21}$$

The coefficients are not given here with the exception of a_4, given as

$$a_4 = m^2(m-1)^2(m+1)^2(C_{55}\varepsilon_{22} + e_{25}^2)C_{22}. \tag{22}$$

The case of $m = 0$ corresponds to axisymmetric vibration, in which $u_\theta = 0$ and all fields are independent of the coordinate θ. This is a specialized case of the more general problem and is not considered here. For the cases considered here, there are six roots to eqn (20), all of which can be found in closed form.

For the case $m \neq 1$, there are typically six distinct roots for α. For $j = 0$, eqn (18) can be solved for the constants $H_r(0)$, $H_\theta(0)$, $H_z(0)$, and $H_\phi(0)$. There are a total of eight roots for α, denoted for each constant by the index k, and hence eight of the constants $H(0,k)$ for each value for k.

For $k = 1, \ldots, 6$, the constants corresponding to $j = 0$ are given by

$$H_r(0,k) = G(k) \tag{23}$$

$H_\theta(0,k) =$

$$\frac{\begin{array}{l}[-e_{25}m(\alpha+1) - e_{12}m\alpha][e_{11}\alpha^2 + e_{12}\alpha - e_{25}m^2] \\ \quad -[-(C_{12}+C_{55})m\alpha - (C_{55}+C_{22})m][-\varepsilon_{11}\alpha^2 + \varepsilon_{22}m^2]\end{array}}{[C_{55}\alpha^2 - (C_{22}m^2 + C_{55}][-\varepsilon_{11}\alpha^2 + \varepsilon_{22}m^2] - [-e_{25}m(\alpha+1) - e_{12}m\alpha][e_{12}m\alpha + e_{25}m(\alpha-1)]} \tag{24}$$

$$H_z(0,k) = 0 \tag{25}$$

$H_\phi(0,k) =$

$$\frac{\begin{array}{l}[e_{12}m\alpha + e_{25}m(\alpha-1)][-(C_{12}+C_{55})m\alpha - (C_{55}+C_{22})m] \\ \quad -[C_{55}\alpha^2 - (C_{22}m^2 + C_{55})][e_{11}\alpha^2 + e_{12}\alpha - e_{25}m^2]\end{array}}{[C_{55}\alpha^2 - (C_{22}m^2 + C_{55})][-\varepsilon_{11}\alpha^2 + \varepsilon_{22}m^2] - [-e_{25}m(\alpha+1) - e_{12}m\alpha][e_{12}m\alpha + e_{25}m(\alpha-1)]} \tag{26}$$

where $G(k)$ are arbitrary constants. For the case $k = 7, 8$ the parameters are computed as $H_r(0,k) = H_\theta(0,k) = H_\phi(0,k) = 0$ and $H_z(0,k) = 1$.

Continuing to collect the coefficients of $r^{\alpha+j-2}$ and setting them to zero results in the following system for any $j > 0$.

$$\begin{bmatrix} F_1 & F_2 & 0 & F_3 \\ F_4 & F_5 & 0 & F_6 \\ 0 & 0 & F_7 & 0 \\ F_8 & F_9 & 0 & F_{10} \end{bmatrix} \begin{Bmatrix} H_r(j) \\ H_\theta(j) \\ H_z(j) \\ H_\phi(j) \end{Bmatrix} = \begin{Bmatrix} F_{11} \\ F_{13} \\ F_{12} \\ F_{14} \end{Bmatrix}. \tag{27}$$

These coefficients depend on the material properties and the values for α, m, N, and j. They are listed in the Appendix.

A sequential solution of this system for each value of j can be constructed using recurrence relations, and results in computation of the constants $H_r(j,k)$, $H_\theta(j,k)$, $H_z(j,k)$, and $H_\phi(j,k)$ in the form

$$\{H_r(j,k);H_\theta(j,k);H_z(j,k);H_\phi(j,k)\} = G(k)\{d_r(j,k);d_\theta(j,k);d_z(j,k);d_\phi(j,k)\}. \quad (28)$$

Substitution of these expressions into eqn (17) yields the final form of the displacement and electrostatic potential as

$$u_r^i(r,\theta,z) = \sum_{m=0}^{\infty}\sum_{n=0}^{\infty} \cos m\theta \sin\frac{n\pi z}{b} \sum_{k=1}^{8} \chi_r^{mn}(i,k)G(i,k) \quad (29)$$

$$u_\theta^i(r,\theta,z) = \sum_{m=0}^{\infty}\sum_{n=0}^{\infty} \sin m\theta \sin\frac{n\pi z}{b} \sum_{k=1}^{8} \chi_\theta^{mn}(i,k)G(i,k) \quad (30)$$

$$u_z^i(r,\theta,z) = \sum_{m=0}^{\infty}\sum_{n=0}^{\infty} \cos m\theta \cos\frac{n\pi z}{b} \sum_{k=1}^{8} \chi_z^{mn}(i,k)G(i,k) \quad (31)$$

$$\phi^i(r,\theta,z) = \sum_{m=0}^{\infty}\sum_{n=0}^{\infty} \cos m\theta \sin\frac{n\pi z}{b} \sum_{k=1}^{8} \chi_\phi^{mn}(i,k)G(i,k) \quad (32)$$

where the functions χ are dependent on geometry, material properties, α, m, N, and k. The corresponding stress and electric displacement fields can be computed with little difficulty, and are not listed here.

When $m = 1$, the coefficient $a_4 = 0$ from eqn (21). Hence there are two repeated roots for α of zero. In this case, the solutions for the displacements and potential appear in a slightly different form from that given in eqn (17). If the first root of zero is denoted as α_1, the solution corresponding to this root is of the form found in eqn (17). A second independent solution can be found by differentiating this solution with respect to α and then letting α go to zero (Srinivas 1974).

For each layer i of the cylinder, the elastic and electric fields are a function of eight constants $G(i,k)$, $k = 1,\ldots,8$. These constants are evaluated by imposing the boundary conditions at the inner and outer surface and the interface conditions between each layer. There are four boundary conditions at each surface, and are imposed on either of the components from the pairs (u_r, σ_{rr}), $(u_\theta, \sigma_{r\theta})$, (u_z, σ_{rz}), and (ϕ, D_r). At each interface, continuity exists for the displacements, potential and radial stress and electric displacement. For example, the continuity condition for the radial displacement u_r can be written as

$$u_r^i|_{r=r_i} = u_r^{i+1}|_{r=r_i}. \quad (33)$$

Similar relations exist for u_θ, u_z, ϕ, σ_{rr}, σ_{rz}, $\sigma_{r\theta}$, and D_r for each layer. There are a total of 8 boundary conditions (four on each surface) and $8(M-1)$ continuity conditions for a total of $8M$ equations. This corresponds to the $8M$ unknown constants $G(i,k)$, $i = 1,\ldots,M$ and $k = 1,\ldots,8$. Imposition of these conditions results in a linear system that can be solved for these constants. Substitution into eqns (28)–(31) yields the final form of the solution for any (r, θ, z) within the cylinder.

NUMERICAL EXAMPLES

Convergence and validation

Several different claims have been made about the rate of convergence of the type of series solution used here. Srinivas (1974) states that the series solution is slowly convergent for the three-dimensional elastic cylinder, with between 80 and 140 terms required for good accuracy. Mirsky (1964) has noted that the power-series expansions converge rapidly for the problem of wave propagation in an infinite elastic cylindrical shell, but did not quantify this statement.

The convergence is tested here using a single layer shell composed of PZT-4 under an

Table 1. Elastic, piezoelectric, and dielectric properties of piezoelectric material

C_{11} (GPa)	115.0
C_{22}	139.0
C_{33}	139.0
C_{12}	74.3
C_{13}	74.3
C_{23}	77.8
C_{44}	25.6
C_{55}	25.6
C_{66}	30.6
$e_{34}(C/m^2)$	12.72
e_{25}	12.72
e_{11}	15.08
e_{12}	−5.08
e_{13}	−5.20
$\varepsilon_{11}/\varepsilon_0$	1300
$\varepsilon_{22}/\varepsilon_0$	1475
$\varepsilon_{33}/\varepsilon_0$	1475

applied radial stress on the outer surface of the form

$$\sigma_{rr}(R_O, \theta, z) = \cos 2\theta \sin \frac{\pi z}{L}. \tag{34}$$

The material properties used are those listed in Table 1 (Berlincourt and co-workers 1964). The geometric parameters are $R_I = 0.005$ m, $R_O = 0.01$ m, and $L = 0.01$ m. The outer and inner surfaces are fixed at zero potential. The inner radial surface is traction free, as is the outer surface with the exception of the σ_{rr} distribution.

Table 2 shows the result of substituting the series solutions into the governing equilibrium and charge evaluations evaluated at $r = R_I$, with the headings of the columns indicating the specific equation. Adequate convergence is achieved after 50 terms. Similar trends exist for other locations within the shell as well as other geometries and boundary conditions. The error for 100 terms is also shown for thinner shells, with a slight increase in error resulting as the shell becomes thin. However, there appears to be little loss in accuracy and the results are still excellent.

To further validate the solution procedure and verify basic trends, an additional example is considered and compared with results found using a semi-analytic finite element methodology similar to that described by Siao *et al.* (1994), from which additional details can be obtained. In this approximate method, the circumferential and axial variations are described by analytic functions and the radial variation is modeled using quadratic finite elements through the thickness of the cylinder. A number of different layers can then be used to describe the thickness dimensions of the laminate.

Table 2. Error in governing equations versus terms in series

	Equation			
Terms	ΣF_r	ΣF_θ	SF_z	div **D**
1	−0.588e3	−0.154e4	0.312e4	−0.304e-6
3	0.223e3	−0.433e3	0.546e3	0.235e-7
5	0.481e3	−0.530e3	0.554e3	0.832e-7
7	0.803e2	−0.469e2	0.413e2	0.904e-8
10	0.116e1	−0.421e0	−0.299e1	0.239e-10
25	−0.310e-11	0.307e-12	−0.272e-12	−0.564e-21
50	−0.224e-24	−0.693e-25	0.546e-25	0.231e-33
100	−0.224e-24	−0.693e-25	0.546e-25	0.231e-33
100 ($R_I = 0.009$)	−0.643e-24	−0.153e-25	0.937e-25	0.581e-33
100 ($R_I = 0.0099$)	−0.234e-22	−0.217e-23	0.465e-23	0.225e-31
100 ($R_I = 0.00999$)	0.144e-21	0.291e-22	−0.321e-22	0.155e-30

Table 3. Comparison of exact field quantities with results from semi-analytic finite element calculation

Layers	$u_r \times 10^{10}$	a. $R_I = 0.05$ $u_\theta \times 10^{10}$	$u_z \times 10^{10}$	ϕ
1	0.12010	−0.22630	0.26473	0.36095
2	0.099622	−0.22331	0.26079	0.36638
4	0.10026	−0.22294	0.26054	0.36625
10	0.10034	−0.22292	0.26050	0.36624
Exact	0.10034	−0.22292	0.26050	0.36624
Layers	$u_r \times 10^{12}$	b. $R_I = 0.009$ $u_\theta \times 10^{11}$	$u_z \times 10^{10}$	ϕ
1	0.83918	−0.78123	0.11667	0.50397
2	0.83289	−0.78450	0.11713	0.50402
4	0.83295	−0.78449	0.11713	0.50402
10	0.83296	−0.78449	0.11713	0.50402
Exact	0.83296	−0.78449	0.11713	0.50402

For this case, we would consider the same cylinder used above with a potential of the form

$$\phi(R_O, \theta, z) = \cos 2\theta \sin \frac{\pi z}{L} \tag{35}$$

applied at the outer surface with the inner surface at R_I fixed at zero potential. Both the inner and outer surfaces of the shell are traction-free. Two inner radii are considered: 0.005 m and 0.009 m, representing a thick and thin shell, respectively. Different numbers of layers or elements are used to model the thickness of the shell: 1, 2, 4, and 10.

The three displacement components and the electrostatic potential at the geometric center of the shell thickness are listed in Tables 3a and 3b. The agreement is excellent, with 4 layers yielding very good accuracy and the results using 10 layers coinciding with the exact solution. From these tables, it is clear that the smaller number of layers results in smaller errors as the shell becomes thin. The potential for the thin shell is close to 0.5, indicating nearly linear behavior. The thick shell departs dramatically from this behavior, as it does even for the purely electrostatic problem. The excellent agreement shown indicates an accurate numerical solution.

Variation of potential

The nature of the electrostatic potential distribution through the cylinder thickness is strongly dependent upon the relative shell thickness. As the radial thickness varies from thin to thick, the distribution goes from nearly linear behavior to strongly nonlinear. Additionally, the influence of piezoelectric coupling varies as the shell thickness changes for a cylinder of fixed outer radius and height. In this example, this influence is studied by considering a single layer shell of PZT-4. The geometric parameters are $L = 0.01$ m and $R_O = 0.01$ m.

The case of imposed surface potentials as used in the previous section in equation (35) is repeated here, with three values of the inner radius considered to vary the thickness of the shell. The strength of the coupling is demonstrated in this example by plotting the parameter s, which is defined as $\phi_c/\phi_n - 1$, with ϕ_c representing the potential for the coupled piezoelectric field and ϕ_n the potential for the electrostatic problem with no piezoelectric coupling (i.e. all $e_{ij} = 0$). The parameter s is measured at $\theta = 0$ and $z = L/4$ and plotted through the shell thickness. This is shown in Fig. 1 for the following values of R_I: 0.0025 (dotted line), 0.005 (dashed line), and 0.009 (solid line). All distributions in this section are plotted through the normalized radial parameter $\bar{R} = (r - R_I)/H$. As the shell thickness becomes thin, there is a smaller difference in the potential for the two cases. For thicker

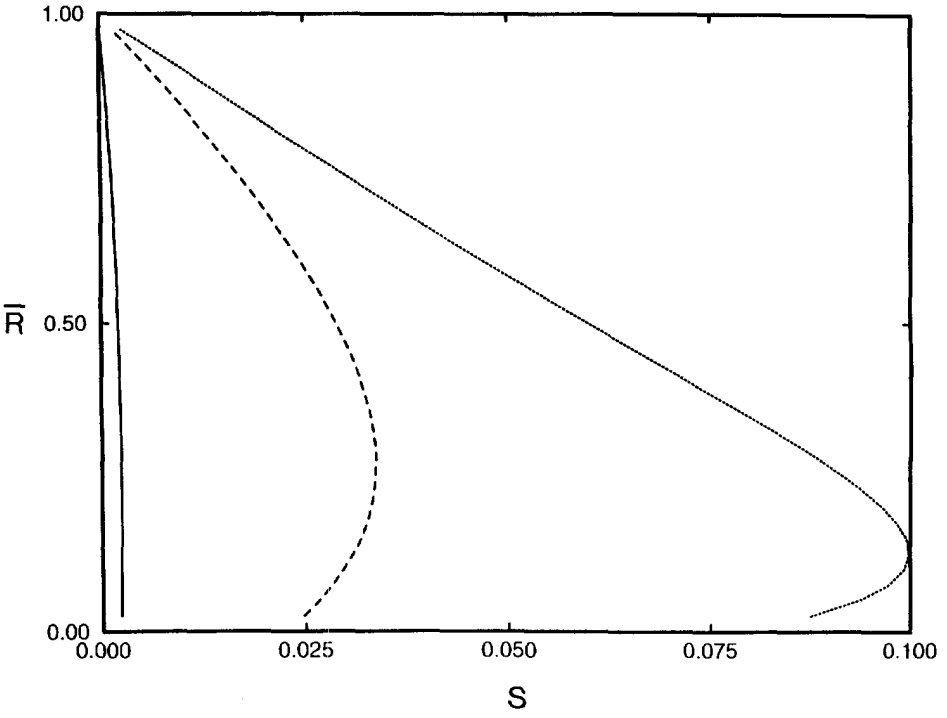

Fig. 1. Difference in electrostatic potential for coupled and uncoupled fields for single layer shell (—: $H = 0.009$, – – –: $H = 0.005$, · · ·: H = 0.0025).

shells, there are larger changes in the potential distribution toward the inner surface, with nearly ten percent difference for the thickest shell. Though not shown, the through-thickness potential distributions for the two thickest shells are highly nonlinear, while the case of $R_I = 0.009$ yields a potential distribution which is nearly linear. This further demonstrates the need to accept the assumption of constant electric field for thin shells only.

A three-layer shell

A three-layer shell under an imposed radial deformation ($m = 2$, $N = 1$, $u_{max} = 1 \times 10^{-8}$) is considered next. Two materials are used. The first is the PZT-4 with the properties listed in Table 1. This material forms the outer and inner layers of the shell. The middle layer is formed of a material with the elastic properties exactly half of the PZT-4 and the piezoelectric and dielectric constants exactly double those of the PZT-4. The purpose of this example is to observe the trends in the fields, particularly near each interface, as the thickness changes relative to the cylinder length.

The length and outer radius of the shell are again fixed at $L = R_O = 0.01$ m. Four total shell thicknesses H are considered and divided into three layers of equal thickness. The properties are those described above. The resulting field distributions are shown in Fig. 2a–f for the values of R_I: 0.0025 (solid line), 0.005 (dotted line), 0.0075 (dashed line), and 0.009 (dot-dashed line).

There is clearly much more variability in the field components for the thicker shells. As the shell becomes thin, both the circumferential and axial displacements tend towards linear behavior through the thickness and the radial displacement tends toward constant behavior. Even for a relatively thick shell ($L/H = 4$) the approximation of linear variation through the thickness may prove to be adequate. The potential distribution shown in Fig. 2d also yields significant breaks in slope across each interface. This is caused by the jump in the elastic and electric properties, and indicates that approximate theories that impose either linear or parabolic behavior through the thickness may not accurately represent the behavior for thicker shells. However, simpler approximations may be sufficient for thin shells.

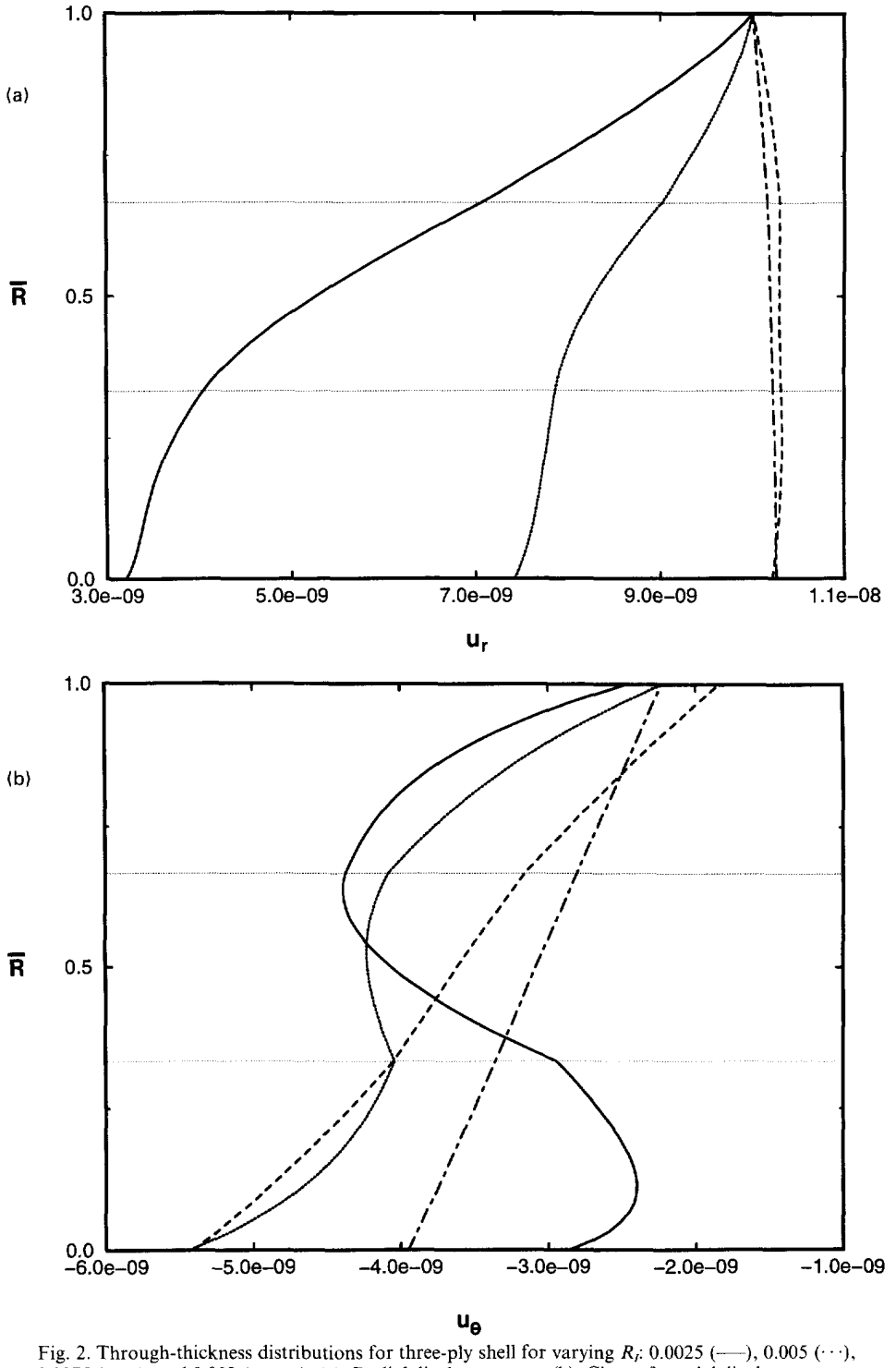

Fig. 2. Through-thickness distributions for three-ply shell for varying R_f: 0.0025 (——), 0.005 (· · ·), 0.0075 (– – –), and 0.009 (· – · – · –). (a) Radial displacement u_r. (b) Circumferential displacement u_θ. (c) Axial displacement u_z. (d) Potential ϕ. (e) Transverse shear stress $\sigma_{r\theta}$. (f) Radial electric displacement D_r.

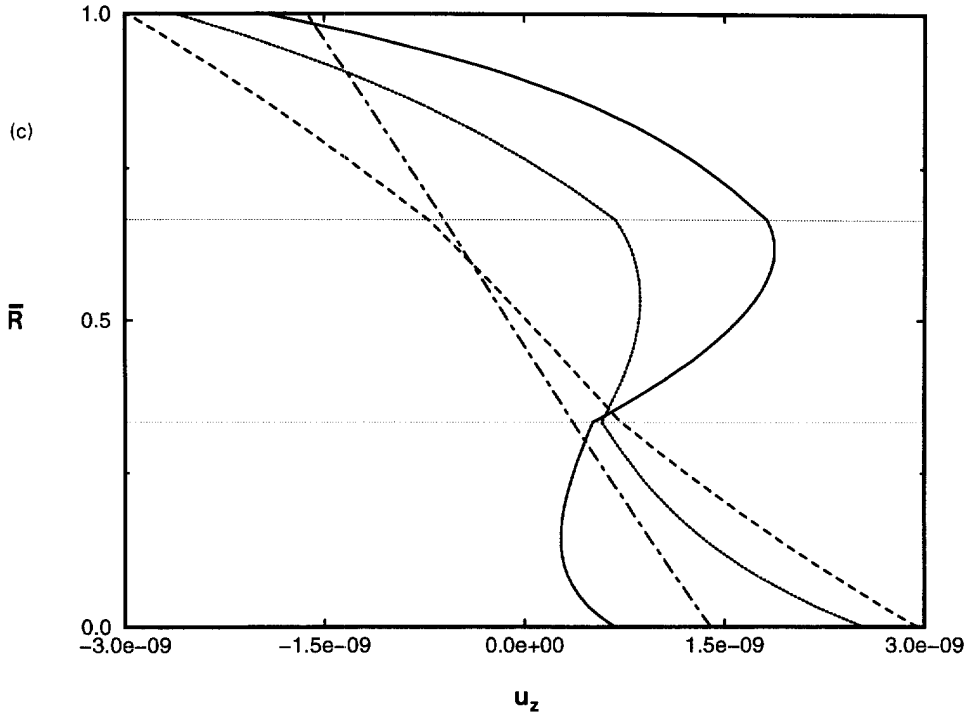

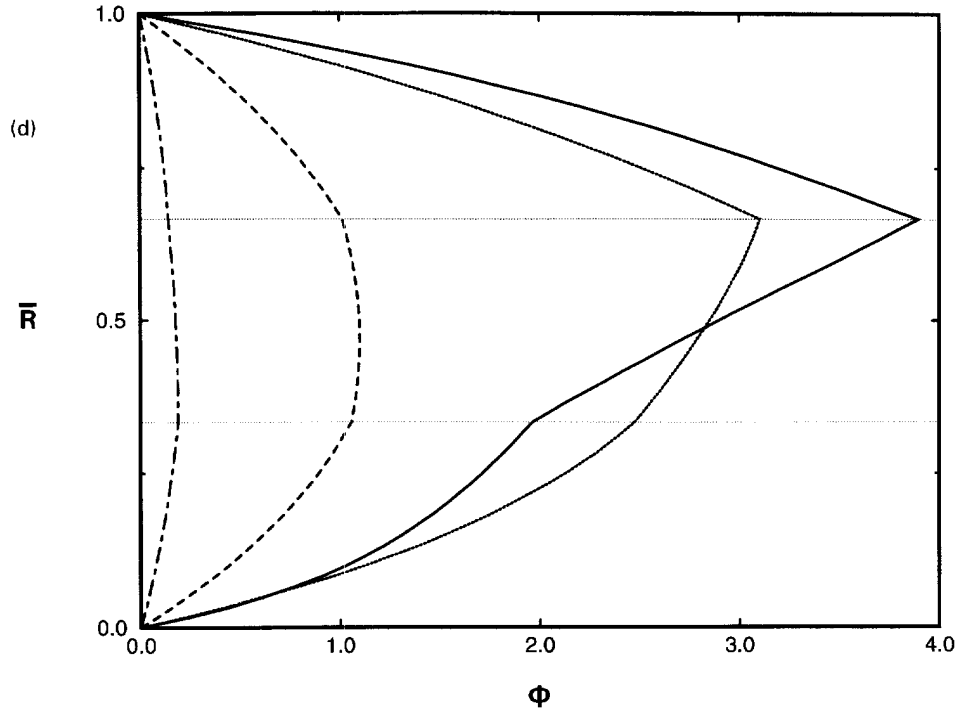

Fig. 2.—*Continued.*

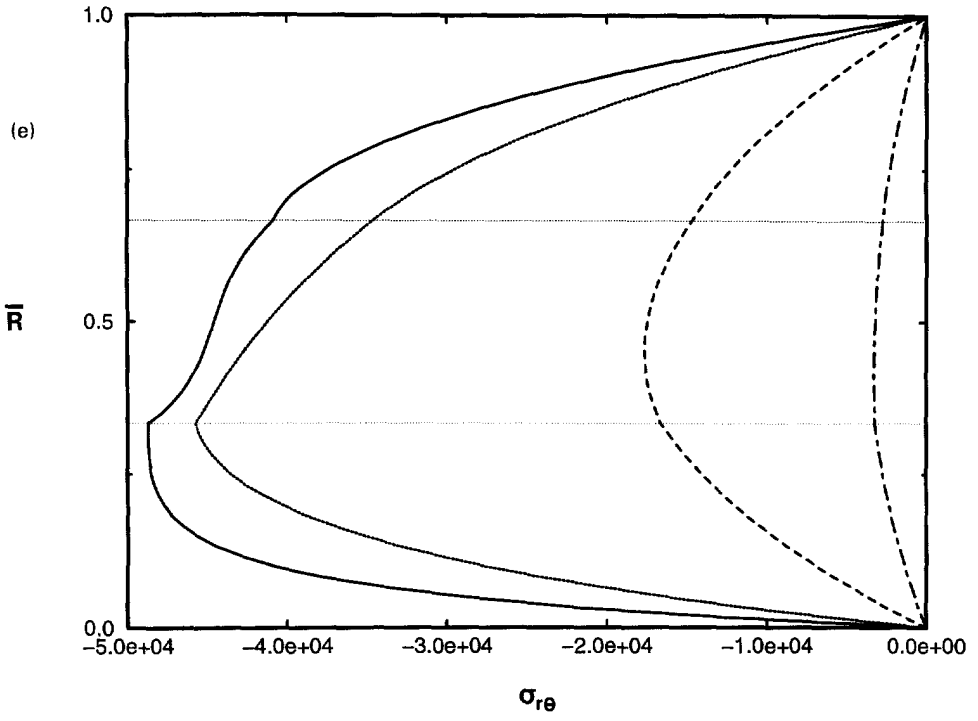

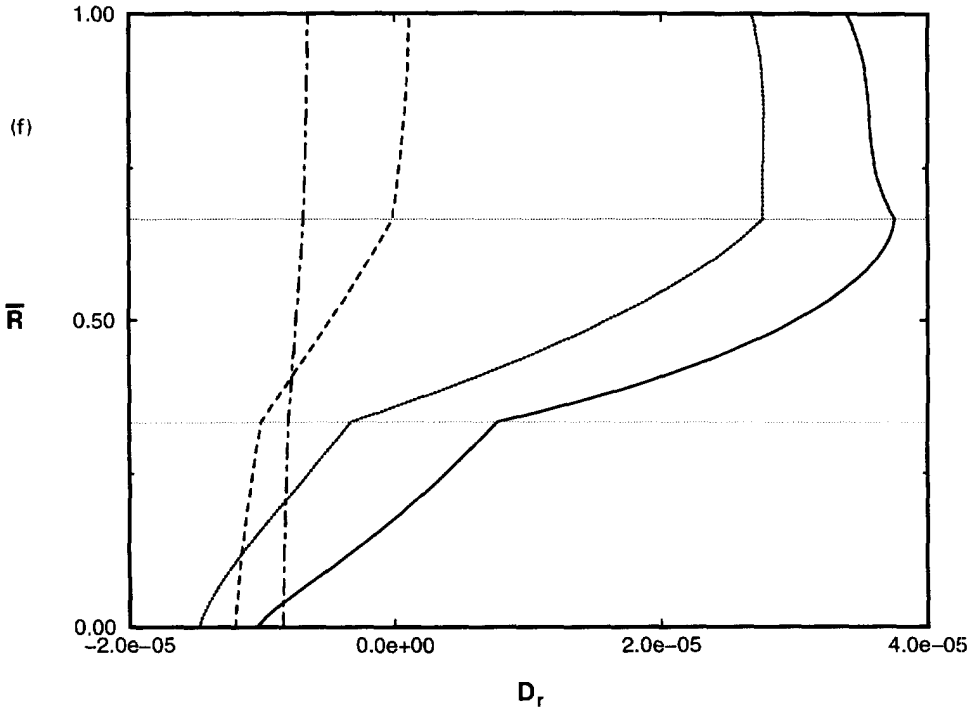

Fig. 2.—*Continued.*

Similar trends are observed for the stress and electric displacement distributions. Figure 2e and f show the distributions for $\tau_{r\theta}$ and D_r, respectively, through the thickness. As the shell becomes thin, the shear stress tends towards parabolic behavior while the electric displacement tends towards constant behavior. Both assumptions are somewhat common in approximate piezoelectric plate theories, and indicate that similar assumptions would be valid for thin piezoelectric shells.

CONCLUSIONS

By extending the procedure of Frobenious as used by Srinivas (1974), exact solutions for the three-dimensional static behavior of laminated piezoelectric cylindrical shells with simple support have been developed. The results compare extremely well with results from a semi-analytic finite element model. For the shells considered in this study, it was found that the assumptions of constant radial displacement and linear circumferential and axial displacement may yield sufficient accuracy for shells with L/H ratios of around 4. For an applied surface potential, the thickness distribution also approaches linear behavior at this same ratio, and parabolic behavior for other forcing conditions with the outer and inner surfaces fixed at ground. The distributions presented here should also provide a basis for comparison for other approximate shell theories.

REFERENCES

Adelman, N. T. and Stavsky, Y. (1975) Vibrations of radially polarized composite piezoceramic cylinders and disks. *Journal of Sound and Vibration* **43,** 37–44.

Berlincourt, D. A., Curran, D. R. and Jaffe, H. (1964) Piezoelectric and Piezomagnetic Materials and their Function in Transducers. In *Physical Acoustics*, Ed. W. P. Mason, Vol. 1, pp. 169–270. Academic Press, New York.

Fung, Y. C. (1965) *Foundations of Solid Mechanics*. Prentice-Hall, Englewood Cliffs, NJ.

Heyliger, P. R. (1994) Static behavior of laminated elastic/piezoelectric plates. *AIAA Journal* **32,** 2481–2484.

Heyliger, P. R. and Brooks, S. P. (1995) Free vibration of piezoelectric laminates in cylindrical bending. *International Journal of Solids and Structures* **32,** 2945–2960.

Heyliger, P. R. and Saravanos, D. A. (1995) Exact free vibration behavior of laminated plates with embedded piezoelectric layers. *Journal of the Acoustical Society of America* **98,** 1547–1557.

Mirsky, I. (1966) Three-dimensional and shell-theory analysis for axisymmetric vibrations of orthotropic shells. *Journal of the Acoustical Society of America* **39,** 549–555.

Mitchell, J. A. and Reddy, J. N. (1995) A study of embedded piezoelectric layers in composite cylinders. *ASME Journal of Applied Mechanics* **62,** 166–173.

Parton, V. Z. and Kudryavtsev, B. A. (1988) *Electromagnetoelasticity*. Gordon and Breach Science Publishers, New York.

Paul, H. S. and Natarajan, K. (1996) Flexural vibration in a finite piezoelectric hollow cylinder of class 6mm. *Journal of the Acoustical Society of America* **99**, 373–382.

Ray, M. C., Bhattacharya, R. and Samanta, B. (1993) Exact solutions for static analysis of intelligent structures. *AIAA Journal* **31,** 1684–1691.

Siao, J. C.-T., Dong, S. B. and Song, J. (1994) Frequency spectra of laminated piezoelectric cylinders. *ASME Journal of Vibration and Acoustics* **116,** 364–370.

Srinivas, S. (1974) Analysis of laminated, composite, circular cylindrical shells with general boundary conditions. NASA TR R-412, NASA Langley Research Center.

Sun, C. T. and Cheng, N. C. (1974) Piezoelectric waves on a layered cylinder. *Journal of Applied Physics* **45,** 4288–4294.

Tiersten, H. F. (1969) *Linear Piezoelectric Plate Vibrations*. Plenum Press, New York.

Tzou, H. S. (1993) *Piezoelectric Shells: Distributed Sensing and Control of Continua*. Kluwer Academic, Norwell, MA.

Xu, K., Noor, A. K. and Tang, Y. Y. (1995) Three dimensional solutions for coupled thermoelectroelastic response of multilayered plates. *Computer Methods in Applied Mechanical Engineering* **126,** 355–371.

APPENDIX

The coefficients F_l given in eqn (26) are expressed as

$$F_1 = C_{11}(\alpha+j)^2 - (C_{55}m^2 + C_{22}) \tag{36}$$

$$F_2 = (C_{12} + C_{55})m(\alpha+j) + (C_{55} + C_{22})m \tag{37}$$

$$F_3 = e_{11}(\alpha+j)^2 - e_{25}m^2 - e_{12}(\alpha+j) \tag{38}$$

$$F_4 = -(C_{12}+C_{55})m(\alpha+j)-(C_{55}+C_{22})m \tag{39}$$

$$F_5 = C_{55}(\alpha+j)^2-(C_{22}m^2+C_{55}) \tag{40}$$

$$F_6 = -e_{25}m(\alpha+j+1)-e_{12}m(\alpha+j) \tag{41}$$

$$F_7 = C_{44}(\alpha+j)^2-C_{66}m^2] \tag{42}$$

$$F_8 = e_{11}(\alpha+j)^2-e_{25}m^2+e_{12}(\alpha+j) \tag{43}$$

$$F_9 = e_{25}m(\alpha+j-1)+e_{12}m(\alpha+j) \tag{44}$$

$$F_{10} = -\varepsilon_{11}(\alpha+j)^2+\varepsilon_{22}m^2 \tag{45}$$

$$F_{11} = -C_{44}N^2H_r(j-2)+[(C_{44}+C_{13})N(\alpha+j-1)+(C_{13}-C_{23})N]H_z(j-1)+e_{34}N^2H_\phi(j-2) \tag{46}$$

$$F_{12} = C_{66}N^2H_\theta(j-2)-(C_{23}+C_{66})mNH_z(j-1) \tag{47}$$

$$F_{13} = -[(C_{44}+C_{13})N(\alpha+j-1)+(C_{44}+C_{23})N]H_r(j-1)-(C_{66}+C_{23})mNH_\theta(j-1) + C_{33}N^2H_z(j-2)-[e_{34}N(\alpha+j)+e_{13}N(\alpha+j-1)]H_\phi(j-1) \tag{48}$$

$$F_{14} = e_{34}N^2H_r(j-2)+[e_{13}N(\alpha+j)+e_{34}N(\alpha+j-1)]H_z(j-1)-\varepsilon_{33}N^2H_\phi(j-2). \tag{49}$$